"Reverse-Uptake" of Zinc-specific Fluorophore in the Prostate by Trans-rectal Florescence Diffuse Optical Tomography

Guan Xu,[1] Daqing Piao,[1*] Chris J. Frederickson,[2] Hamid Dehghani [3]
[1] *School of Electrical and Computer Engineering, Oklahoma State University*
Stillwater, OK, 74078-5032, USA
[2] *Andro Diagnostics Inc., Houston, TX, 77034, USA*
[3] *School of Computer Science, University of Birmingham, Birmingham, B15 2TT, UK*
**Corresponding Author: daqing.piao@okstate.edu*

Abstract: Using fluorophore specific to zinc, a well-established prostate cancer marker, to detect prostate cancer will be challenged by the "reverse-uptake" of the fluorophore. A sensitivity-adapted reconstruction method may improve the target recovery in axial-imaging geometry.

OCIS codes: (170.7230) Urology; (170.6960) Tomography; (170.3010) Image reconstruction techniques; (170.7230) Spectroscopy, fluorescence and luminescence

1 Introduction

Prostate cancer (PCa) is the second commonly diagnosed cancer and the leading cause of cancer death in American men. When the suspicion of PCa is raised, either by elevated serum level of prostate-specific antigen (PSA) and abnormal digital rectal examination (DRE), the patient often choose to undergo the trans-rectal ultrasound (TRUS) guided prostate biopsy, which has evolved to the standard procedure in prostate cancer diagnosis. However, the inability of ultrasound imaging technique to fully discern the benign and malignant tissue leads to the excessive biopsy cores, which is further complicated by the multi-focal involvement of PCa [1]. Improving the accuracy of imaging guidance thereby reducing unnecessary biopsy cores has become one of the critical needs in PCa detection and management. A number of alternative imaging modalities are under investigation toward more accurate differentiation of malignant from benign tissue in prostate [2]. Among these alternative prostate imaging methods, a transrectal diffuse optical tomography (DOT) approach has demonstrated detecting the intrinsic near-infrared (NIR) chromophores in prostate that have different attenuation cross-sections in the malignant and benign tissue environments [3]. A natural extension of trans-rectal DOT is detecting molecular or ionic activities specific to PCa that could further improve the sensitivity and specificity of detection.

Zinc is a well-established metabolic marker of PCa [4]. Benign prostate tissues secret zinc in the form of Zn3Citrate2 and zinc has a concentration of approximately 10mM in prostatic fluid. In cancerous prostate tissue the zinc-secretion is terminated, resulting in five to ten folds of reduced level of zinc in the associated prostatic fluid. A zinc-specific near-infrared fluorophor is being developed by Andro Diagnostics, Inc, Houston, TX. Based on the hypothesis that the concentration of the administered zinc-tagged fluorophor is proportional to that of the free zinc in the prostate, using this approach to detect PCa will face the "reverse-uptake" challenge-----that is having weak or no uptake of the fluorophore in the cancer foci while having rich or strong uptake of the fluophore in the peripheral benign tissue. This "reverse-uptake" constitutes a reconstruction challenge that is different from the previously encountered fluorescence diffuse optical tomography (FDOT) scenarios. In axial-imaging trans-rectal FDOT geometry, the reconstruction will be further challenged by the sensitivity that is strongly dependent upon the depth.

This paper discusses the "reverse-uptake" reconstruction in an axial-imaging geometry. A reconstruction mesh adapted to the depth sensitivity and the indicated azimuthal location of a single target is implemented. The preliminary simulation study demonstrates that the method could improve the recovery of a "reverse-uptake" target.

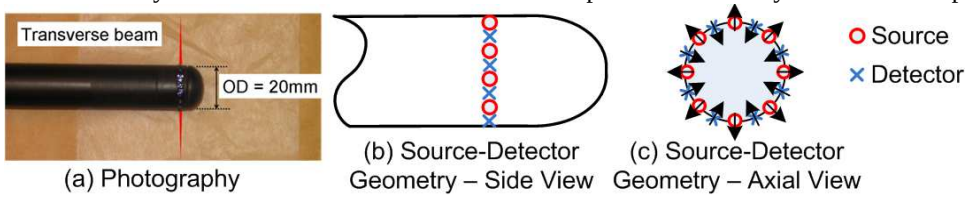

Fig. 1 A 20-mm diameter, 8 sources by 8 detectors axial-imaging trans-rectal applicator

2 Methods and Materials

The simulation study is based on a 20mm diameter axial transrectal probe, as shown in Fig. 1, that we developed [5]. The 8 source and 8 detector channels are interspersed and evenly distributed around the axial cross-section.

The simulation study utilized 2-dimensional finite element method for steady-state photon diffusion and fluorescence emission in the axial-imaging plane as:

$$\nabla^2 U_x(\vec{r}) - \frac{\mu_{ax}}{D_x} U_x(\vec{r}) = -\frac{S(\vec{r})}{vD_x}, \quad \nabla^2 U_m(\vec{r}) - \frac{\mu_{am}}{D_m} U_m(\vec{r},\omega) = -\frac{U_x(\vec{r}) \cdot \eta\mu_{af}}{vD_m} \tag{1}$$

where subscripts "x" denotes excitation and "m" denotes emission. The diffusion coefficient $D_{x,m}=1/[3(\mu_{ax,m+}\mu_s'_{x,m})]$, where $\mu_{ax,m}$ and $\mu_s'_{x,m}$ are absorption and scattering coefficients for excitation and emission band, respectively. The η and μ_{af} are the quantum efficiency and the absorption coefficient of the fluorophore respectively, the product of which is defined as the fluorescence yield. The forward solver implements the Robin type boundary condition as:

$$U_{x,m}(\vec{r}_0) + 2D_{x,m} A\hat{n}_0 \cdot \nabla U_{x,m}(\vec{r}_0) = 0 \tag{2}$$

where $\vec{r}_0$ is the boundary nodes, $\hat{n}_0$ is the outward normal vector of the boundary and A is a coefficient related to the refractive index mismatch. The Levernberg-Marquart algorithm is implemented to the inverse solver as:

$$x_{k+1} = x_k + \alpha \cdot [J^T(x_k)J(x_k) + \lambda I]^{-1} J^T(x_k)\Delta v(x_k) \tag{3}$$

where α in the range of [0,1] is a damping factor , J is the sensitivity matrix and Δv is the forward projection error. When only the contrast of florescence yield is considered, the unknown values x represents the $\eta\mu_{af}$ term in equ.(1).

For all the simulations conducted in this work, only the contrast of fluorescence yield is considered, by setting η=0.1, μ_{af}=0.005 for the target and η=0.1, μ_{af}=0.01 for the background. Other parameters are set as: $\mu_{ax,m}$=0.01mm^{-1}, $\mu_s'_{x,m}$=1mm^{-1} and A=2.82. A white noise of 1% is added to the simulated forward data.

3 Results

3.1 Region-wise reconstruction

The region-wise reconstruction is first simulated to assess the accuracy of recovering a "reverse-uptake" fluorescence target with accurate *prior* knowledge of the target spatial information, including shape, size, and depth. Supposing that the accurate profile of the structures within the imaging volume can be accurately extracted from the complementary imaging modality such as TRUS and MRI, and assuming homogeneity of optical properties and fluorescence yield within each segmented region, the so called "hard" *a priori* reconstruction algorithm [5] is modified for FDOT.

Simulation approaches are shown in Fig.2. Targets with the radius shown in Fig.2 (b) and (c) are set at a depth from the source-detector array at an increment of 5mm (Fig. 2(a)). Notice that for r>5mm, the round target at 5mm depth is interfered by the inner boundary of the imaging volume, therefore the target shape must be modified at that specific depth. The comparison of the recovered fluorescence yield within the target region is given in Fig.2(c).

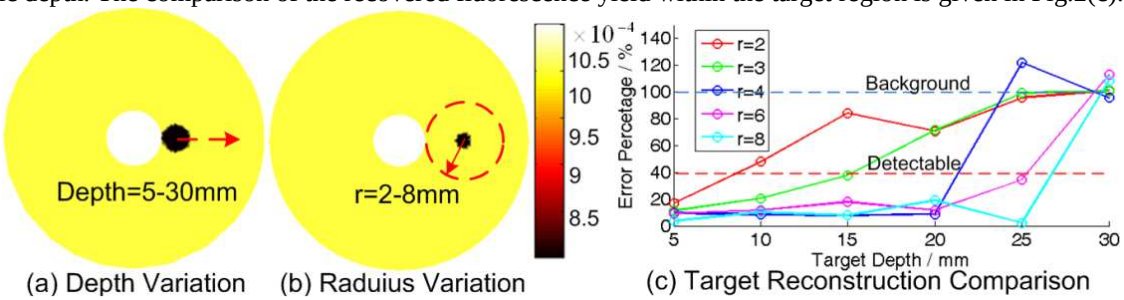

Fig.2 Region-wise reconstruction

We set a 40% error tolerance as the threshold for the target recovery. It is observed that, (1) The detectable depth increases as the target size increases; (2) the imaging depth of 15-20mm is attainable for this imaging geometry for most of the target sizes; (3) the recovered fluorescence yields of all targets converge to the background ((0.001-0.0005)/0.0005=100%) values at 30mm depth, which is the limit of the detection.

3.2 Piece-wise reconstruction

The above region-wise reconstruction is only an "ideal" case. Piecewise reconstruction is more practical because of the lack of accurate target information when TRUS is used to visualize the prostate morphology. When no spatial *prior* information of the target can be implemented, the axial transrectal imaging will be challenged by the depth-dependent sensitivity inherent to the side-firing reflective imaging geometry. To compensate the sensitivity distribution, an adaptive mesh is implemented [6]. As is shown in Fig. 3(a)(c), with the notion that the uniformity of the product of relative sensitivity value and the element size within the imaging volume contributes to the correction of depth-dependent sensitivity [7], the element sizes are adjusted according to the depth-sensitivity. Further, since in this axial-imaging geometry, when there is only one target, the approximate azimuthal location and dimension may be indicated by the change of the signal with respect to the baseline, the approximate target area can be estimated

BSuD19.pdf

and thereby segmented into denser elements. Fig.3 shows the meshes generated with: (b) uniform element size (c) depth-adapted elements, and (d) depth and azimuth adapted elements.

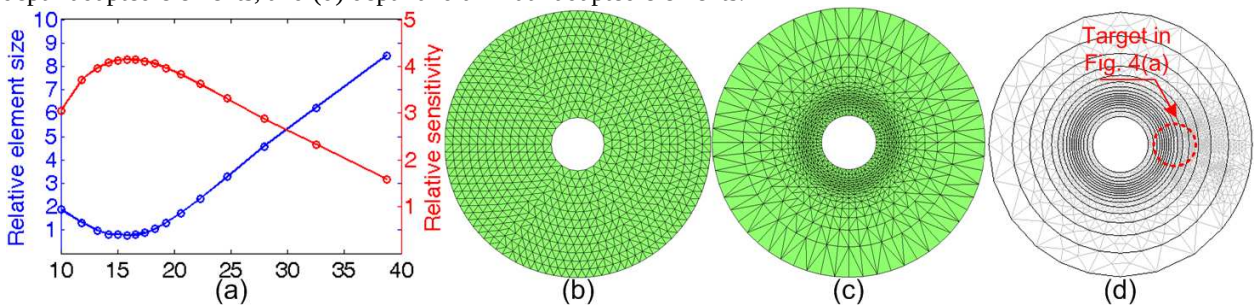

Fig. 3 Adaptive meshes (a) element-size vs. depth-sensitivity; (b) uniform mesh; (c) depth-adapted elements; (d) depth and azimuth-adapted elements corresponding to Fig.4(a)

The efficacy of the adaptive mesh elements shown in Fig. 3 is tested in Fig. 4(a) for a 7mm radius target of η=0.1 and μ_{af}=0.005 at a depth of 20mm. The results in Fig. 4(b)-(d) demonstrate that the depth-and-azimuth adapted mesh slightly outperforms the depth-adapted mesh, and the depth-adapted meth significantly outperforms the uniform mesh, in terms of the recovered optical properties.

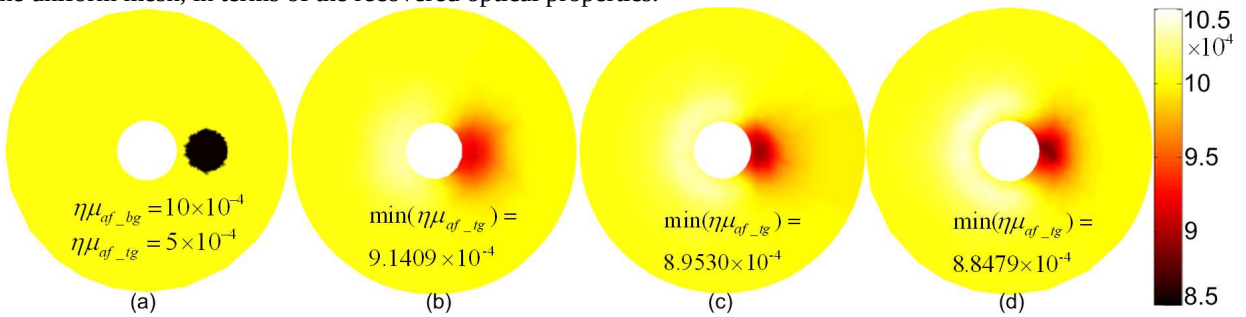

Fig.4 Piece-wise reconstruction (a) target setting (b) uniform mesh; (c) depth-adapted mesh; (d) depth and azimuth-adapted mesh

4 Conclusions and Future Challenges

"Reverse-uptake" will be associated with using zinc-specific fluorophore to detect PCa, which is further challenged by the depth-dependent sensitivity. This initial study demonstrated that the 20mm probe geometry may detect a negative contrast of fluorescence yield at a depth up to 20mm. Further, adaptive mesh has shown improving the target recovery. However, recovery of the correct depth of the target is still problematic, and there are artifacts associated with all methods studied above. The in vivo imaging situation will be further challenged by many factors, such as the optical heterogeneities of the prostate, autofluorescence, and inaccuracy of steady-state detection.

But nonetheless, this study shall provide an insight to how to improve the detection of deeper target in axial trans-rectal imaging geometry, which may be extended to sagittal imaging geometry. Once the zinc-specific NIR fluorophore is developed, experimental studies may help examine and optimize the reconstruction approaches.

References

[1] A. M. Wise, T. A. Stamey, J. E. McNeal, and J. L. Clayton, "Morphologic and clinical significance of multifocal prostate cancers in radical prostatectomy specimens," Urology **60**, 264-269 (2002).
[2] D. Piao, K. E. Bartels, Z. Jiang, G. R. Holyoak, J. W. Ritchey, G. Xu, C. F. Bunting, G. Slobodov, "Alternative trans-rectal prostate imaging: A diffuse optical tomography method," IEEE Journal of Selected Topics in Quantum Electronics, "Biophotonics 2" Special Issue, invited paper, in press (will appear in Jul/Aug., 2010).
[3] Z. Jiang, G. R. Holyoak, K. E. Bartels, J. W. Ritchey, G. Xu, C. F. Bunting, G. Slobodov, D. Piao, "In vivo trans-rectal ultrasound-coupled near-infrared optical tomography of a transmissible venereal tumor model in canine pelvic canal, " J. of Biomed. Opt. Lett. **14**, 030506-1-030506-3 (2009).
[4] V. Ye. Zaichick, T. V. Sviridova, S. V. Zaichick, "Zinc concentration in human prostatic fluid: normal, chronic prostatitis, adenoma and cancer," Int. Urol. Nephrol. **28**, 687-694 (1996).
[5] G. Xu, D. Piao, C. H. Musgrove, C. F. Bunting, and H. Dehghani, "Trans-rectal ultrasound-coupled near-infrared optical tomography of the prostate Part I: Simulation," Opt. Exp. **16**, 17484–17504 (2008).
[6] A. Borsic, R. Halter, Y. Wan, A. Hartov and K. D. Paulsen, "Sensitivity study and optimization of a 3D electric impedance tomography prostate probe," Physiol. Meas. **30**, S1-S18 (2009).
[7] M. Huang, T. Xie, N. Chen and Q. Zhu, "Simultaneous reconstruction of absorption and scattering maps with ultrasound localization: feasibility study using transmission geometry," Appl. Opt. **42**, 4102-4114 (2003).